ADDED DRAG ON ACOUSTIC LINERS IN PRESENCE OF GRAZING TURBULENT FLOW AND ACOUSTIC WAVES

ADDED DRAG ON ACOUSTIC LINERS IN PRESENCE OF GRAZING TURBULENT FLOW AND ACOUSTIC WAVES

Angelo Paduano*, Francesco Avallone, Francesco Scarano
Department of Mechanical and Aerospace Engineering (DIMEAS), Politecnico di Torino
Corso Duca degli Abruzzi, 24, 10129 Torino, Italy
angelo.paduano@polito.it

ABSTRACT

Very large eddy simulations are performed to investigate the aerodynamic penalty of wall-mounted acoustic liners in a turbulent channel flow with a centerline Mach number of 0.32. Two liner geometries, differing in orifice-edge shape, are examined both without acoustic forcing and under incident plane acoustic waves with frequencies between 0.8 and 2.0 kHz and sound pressure levels of 130 and 145 dB. Relative to the smooth-wall baseline, the liner alone produces a substantial drag increase, ranging from about 27% for the sharp-edged configuration to about 42% for the chamfered one. At 130 dB, the drag remains close to the flow-only condition, whereas at 145 dB it increases further, reaching up to about 53% above the smooth-wall case. The drag increase is associated with amplified wall-normal oscillatory flow through the orifices, which enhances near-wall momentum exchange and intensifies the velocity deficit downstream of the liner. These effects are reflected in the downward shift of the mean velocity profiles in wall units, consistent with the observed drag increase.

INTRODUCTION

Acoustic liners are a key technology for reducing fan noise in modern aircraft engines. In Ultra-High Bypass Ratio (UHBR) engines, the fan has become the dominant noise source, producing both tonal components at the blade-passing frequency and broadband contributions from rotor/stator interaction. Conventional liners, typically consisting of a perforated facesheet backed by a cavity and rigid plate, are designed to dissipate acoustic energy (Tam & Kurbatskii, 2000) but are not optimized for aerodynamic performances. In real engine conditions, liners operate simultaneously under grazing turbulent flow and incident acoustic waves. The intricate coupling between acoustic waves and turbulent flow within the orifice has been recently described by Paduano *et al.* (2025).

While acoustic liner attenuation properties have been extensively studied, their aerodynamic penalties are less well understood. Tam *et al.* (2014) first reported that strong tonal excitation could enhance drag. Jasinski & Corke (2020) experimentally investigated a turbulent boundary layer grazing over an acoustic liner in the presence of acoustic forcing. Their measurements, obtained using two-component hot-wire anemometry, revealed an enhancement of sweep and ejection events due to the high-amplitude acoustic waves, which was associated with an increase in drag.

Bento *et al.* (2022) showed that boundary-layer impingement on the downstream edge of the perforations induces a pressure force inside the cavity, thereby modifying the mean drag balance. Howerton & Jones (2016) conducted experiments in NASA's GFIT facility under grazing flow and acoustic excitation, reporting drag increments between 10% to 350% relative to a smooth wall. The scatter in the results emphasised a strong dependence on geometric parameters such as orifice diameter, face sheet porosity, and thickness.

Shahzad *et al.* (2023*b*) performed direct numerical simulations of channel flow with wall-mounted acoustic liners in the absence of acoustic forcing. They reported a drag increase of approximately 70% compared to a smooth wall, attributed to a transition toward a fully rough regime in which pressure drag becomes dominant. The authors also proposed a scaling for the downward shift of the logarithmic region of the mean velocity profile in wall units, ΔU^+, based on the inverse of the Forchheimer coefficient. A subsequent study by the same authors (Shahzad *et al.*, 2025) incorporated acoustic forcing into the drag analysis. Their results indicated that the introduction of acoustic waves at 150 dB leads to negligible changes in both drag and ΔU^+.

However, most studies addressing increased drag on acoustic liners, whether experimental or numerical, are conducted at friction Reynolds numbers Re_τ significantly lower than those representative of aircraft nacelles (approximately 4200). As a result, their conclusions are restricted to flow regimes where large-scale motions and inner–outer layer interactions remain relatively weak (de Giovanetti *et al.*, 2016). This limitation may obscure the potential influence of acoustic waves on the drag penalty.

Furthermore, these studies do not include a systematic variation of the incident acoustic forcing. In particular, a comprehensive parametric investigation exploring the effects of acoustic wave amplitude and frequency on drag and ΔU^+ is still lacking in the literature. Such an analysis would enable a more accurate characterisation of roughness behaviour in the presence of acoustic excitation.

The objective of the present work is therefore to investigate, through high-fidelity very large eddy simulations at a realistic Reynolds number, the contribution of plane acoustic waves with varying amplitudes to the aerodynamic drag over an acoustic liner. By explicitly linking acoustic forcing to drag mechanisms, this study aims to provide new insights into the coupled aeroacoustic response of liners, ultimately supporting the design of solutions that balance noise attenuation with acceptable aerodynamic penalties.

1 METHODOLOGY

1.1 Numerical solver

The simulations are performed with the commercial solver 3DS Simulia PowerFLOW (v6), which is based on the Lattice Boltzmann Method (LBM) and employs the D3Q19 lattice model (He & Luo, 1997). A Very Large Eddy Simulation (VLES) approach is adopted, resolving the large turbulent scales while accounting for sub-grid effects through an effective relaxation time derived from renormalization group theory (Yakhot & Orszag, 1986). The solver employs a turbulent wall model that dynamically accounts for the effects of pressure gradients (PGE-WM) (Texeira, 1998).

1.2 Numerical domain

The computational domain, shown in Fig. 1, reproduces the UFSC experimental facility (Bonomo *et al.*, 2022). The liner is mounted on the upper wall of a rectangular duct. Two liner geometries are considered, both consisting of 22 cavities and eight orifices per cavity. Each cavity has a square cross-section of side $l = 9.90$ mm and depth $h = 38.10$ mm. The facesheet has a thickness $\tau = 0.64$ mm, and the cavities are separated by partition walls of width $w_p = 2.53$ mm. The key difference lies in the shape of the orifice edges: one configuration features sharp edges, while the other employs chamfered edges as depicted in Figure 1. This modification results in different effective diameters at the grazing-flow interface, equal to $d = 1.00$ mm and $d = 1.20$ mm, respectively. While both geometries share the same internal diameter $D = 1.00$ mm. These variations are representative of realistic manufacturing tolerances, such as those arising from additive manufacturing processes. As a consequence, the two configurations exhibit different porosities, equal to 6.4% and 9.2%, respectively.

The coordinate system is defined as follows: the streamwise direction is x, the wall-normal direction is y, and the spanwise direction is z. The instantaneous velocity components are u', v', and w', with their time-averaged counterparts U, V, and W, and fluctuation components u, v, and w.

To promote boundary-layer transition, a zig-zag trip (0.24 mm high, 1.95 mm long) is placed upstream of the liner at $x = -1872$ mm. Quasi-anechoic outlet conditions are enforced by exponentially increasing the fluid viscosity within sponge layers, while periodic boundary conditions are applied on the lateral walls.

A multi-resolution lattice grid is used, with six overset meshes. The finest resolution is applied to the facesheet, orifices, and upper portion of the cavities, with a minimum grid spacing of $\Delta x = \Delta y = \Delta z = 0.0234$ mm, corresponding to approximately 50 voxels per orifice diameter.

1.3 Test matrix

The grazing flow corresponds to a centreline Mach number of $M = 0.32$ and a friction Reynolds number $Re_\tau \approx 3600$. To establish reference conditions, two preliminary simulations were performed: a smooth-wall baseline and a lined-wall case without acoustic excitation. After convergence of the hydrodynamic solution, harmonic acoustic waves were superimposed on the flow at selected frequencies. Two acoustic excitation levels, 130 dB and 145 dB, were investigated. It is worth noting that the chamfered-orifice configuration is expected to provide improved acoustic energy dissipation compared to the sharp-edged geometry Avallone *et al.* (2026). The complete test matrix is summarised in Table 1.

1.4 Drag evaluation

In order to quantify the additional drag induced by the presence of the liner, the static pressure was recorded at two streamwise locations, $x = 0$ (upstream of the liner) and $x = L$ (downstream of the liner), across the full height of the channel. The resulting pressure profiles were integrated to obtain the streamwise pressure gradient, which was then used to estimate the wall shear stress as $\tau_w = -h\frac{dp}{dx}$. The skin-friction coefficient was subsequently calculated as $C_f = \tau_w/(1/2\rho U_b^2)$,

Table 1. Summary of the numerical simulations.

case	SPL [dB]	M	f [kHz]
smooth	-	0.32	-
sharp	-	0.32	-
chamfered	-	0.32	-
sharp	130	0.32	0.8, 1.4, 2.0
sharp	145	0.32	0.8, 1.4, 2.0
chamfered	130	0.32	0.8, 1.4, 2.0
chamfered	145	0.32	0.8, 1.4, 2.0

with U_b representing the bulk velocity. The friction velocity, U_τ, is computed from the wall shear stress as $U_\tau = \sqrt{\tau_w/\rho}$

1.5 Forchheimer coefficient

To characterise the inertial resistance of the perforated facesheet to wall-normal flow, the Forchheimer coefficient α_y was introduced. The α_y coefficient was estimated using the empirical formula proposed by Idelchik (1986):

$$\alpha_y = \frac{1}{2\sigma^2\tau}\left[0.5 + 0.24(1-\sigma)^{3/2} + (1-\sigma)^2\right], \qquad (1)$$

where σ is the porosity. In the present study, σ was computed as the ratio between the total open orifice area and the projected liner surface area. The coefficient was then expressed in viscous units as

$$\alpha_y^+ = \alpha_y \frac{\nu}{u_\tau}, \qquad (2)$$

where u_τ is the friction velocity and ν is the kinematic viscosity.

2 RESULTS

2.1 Added drag

In Figure 2(a), the total skin-friction coefficient for a channel flow is reported as a function of the bulk Reynolds number. The smooth-wall baseline shows good agreement with both semi-empirical correlations and the experimental data of Schultz & Flack (2013), thereby validating the present numerical setup.

When the lined surface is introduced, the skin-friction coefficient increases significantly. This increase is more pronounced for the chamfered-orifice configuration, highlighting that even small geometric modifications lead to changes in the surface porosity and substantial changes in drag. The relative increase with respect to the smooth-wall baseline is reported in Figure 2(b) as a function of the forcing SPL at fixed $f = 1400$ Hz, and in Figure 2(c) as a function of the forcing frequency. The dashed line represents the lined case without acoustic forcing, which is therefore independent of frequency. In this configuration, the skin-friction coefficient is approximately 23% higher than the smooth case for sharp-edged orifices and up to 42% higher for chamfered orifices, in agreement with the values reported by Shahzad *et al.* (2023*b*) without acoustic excitation.

When acoustic forcing is applied, an additional increase in drag is observed. At 130 dB increases by up to 27% and 43% for the sharp-edged and chamfered configurations, respectively. At 145 dB, however, the effect becomes significant, with the skin-friction coefficient increasing by nearly

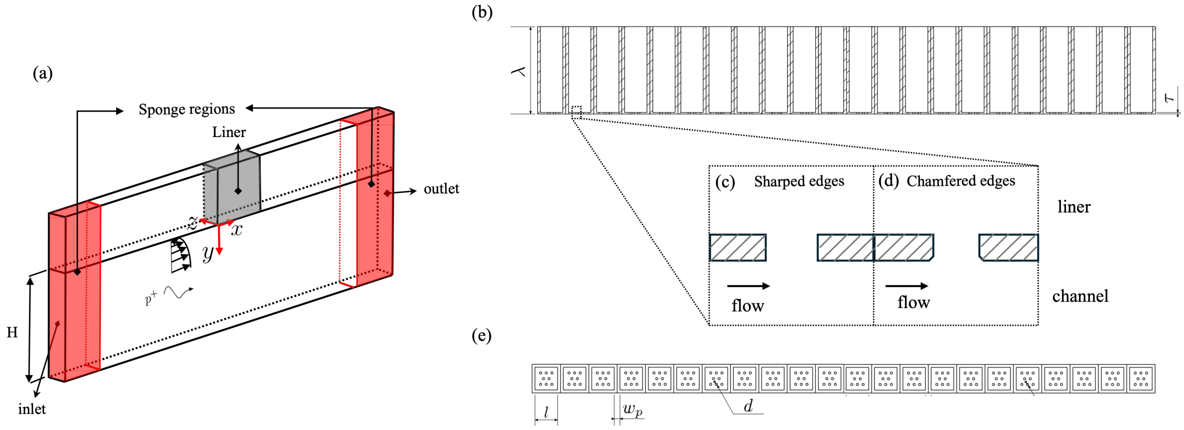

Figure 1. Numerical setup: (a) channel with a lined wall, (b) liner arrangement with twenty-two cavities, (c) detailed view of a cavity with sharp-edged orifices, (d) detailed view of a cavity with chamfered orifices, and (e) wall-normal view of the liner surface.

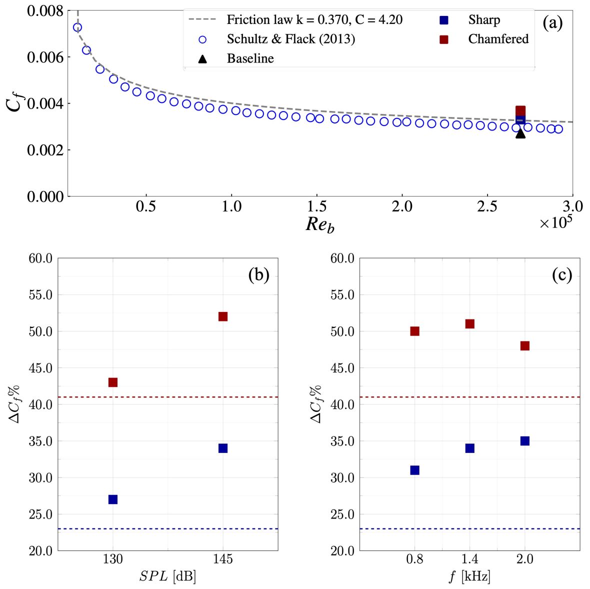

Figure 2. (a) Total skin-friction coefficient as a function of bulk Reynolds number. (b) Relative drag increase compared to the smooth-wall baseline as a function of forcing SPL. (c) Relative drag increase compared to the smooth-wall baseline as a function of forcing frequency. The dashed lines represent the drag increase for the sharp and chamfered configuration without acoustic forcing.

35% and 53% for the sharp-edged and chamfered configurations, respectively. For a fixed SPL of 145 dB, the skin-friction coefficient also exhibits a frequency dependence. The sharp-edged configuration shows a monotonic increase with frequency, reaching a maximum at 2 kHz, whereas the chamfered configuration exhibits a peak around 1.4 kHz. This difference might be associated with the sensitivity of the liner resonance to the orifice geometry, particularly in the presence of grazing flow. The chamfered configuration modifies the effective mass and inertial response of the oscillating fluid within the orifices, thereby shifting the resonance condition and altering the coupling between the acoustic field and the grazing flow. Consistent with acoustic measurements, the resonance frequency of the chamfered geometry is approximately 1900 Hz, whereas that of the sharp-edged configuration is around 1700 Hz. As a result, the frequency dependence of the drag differs between the two geometries (Paduano *et al.*, 2026).

2.2 Orifice-resolved flow topology

To better understand the reasons for the drag increase, the modifications of the in-orifice flow topology and the turbulence structures induced by the liner and acoustic forcing are analysed. The contours of the standard deviation of the streamwise and wall-normal velocity components are shown in Figure 3.

The increase in drag can be attributed to changes in the flow topology both within and above the liner orifices. The presence of the liner enhances streamwise velocity fluctuations in the near-wall region and generates strong wall-normal velocity fluctuations inside the orifices. The flow enters the orifice primarily from the downstream half and impinges on the downstream corner. As reported by Bento *et al.* (2022), this mechanism contributes to pressure drag generation in the absence of acoustic forcing.

At low acoustic forcing (130 dB), the modifications to the flow topology remain limited, and the flow closely resembles the unforced case, which explains the modest increase in drag. In contrast, at 145 dB, a significant amplification of both streamwise and wall-normal fluctuations is observed. This behaviour is associated with periodic ejection and ingestion of fluid through the orifices (Scarano *et al.*, 2024; S. *et al.*, 2023), driven by the acoustic pressure field. These oscillatory motions induce additional fluid transport within the orifice, thereby intensifying the flow impingement on the downstream corner.

Moreover, the acoustic-induced motion alters the near-wall flow downstream of the orifice (see Figures 3 g–h), promoting enhanced momentum exchange between the near-wall region and the outer flow. This process effectively increases turbulent mixing. Such enhanced mixing and stronger inner-outer layer interactions are known to contribute to increased pressure drag over rough surfaces (Chung *et al.*, 2021), providing a physical explanation for the observed drag increase under strong acoustic forcing.

Finally, it is worth noting that the acoustic-induced motion and its impact on the downstream near-wall region are further amplified in the chamfered configuration compared to the sharp-edged one. This observation is consistent with the

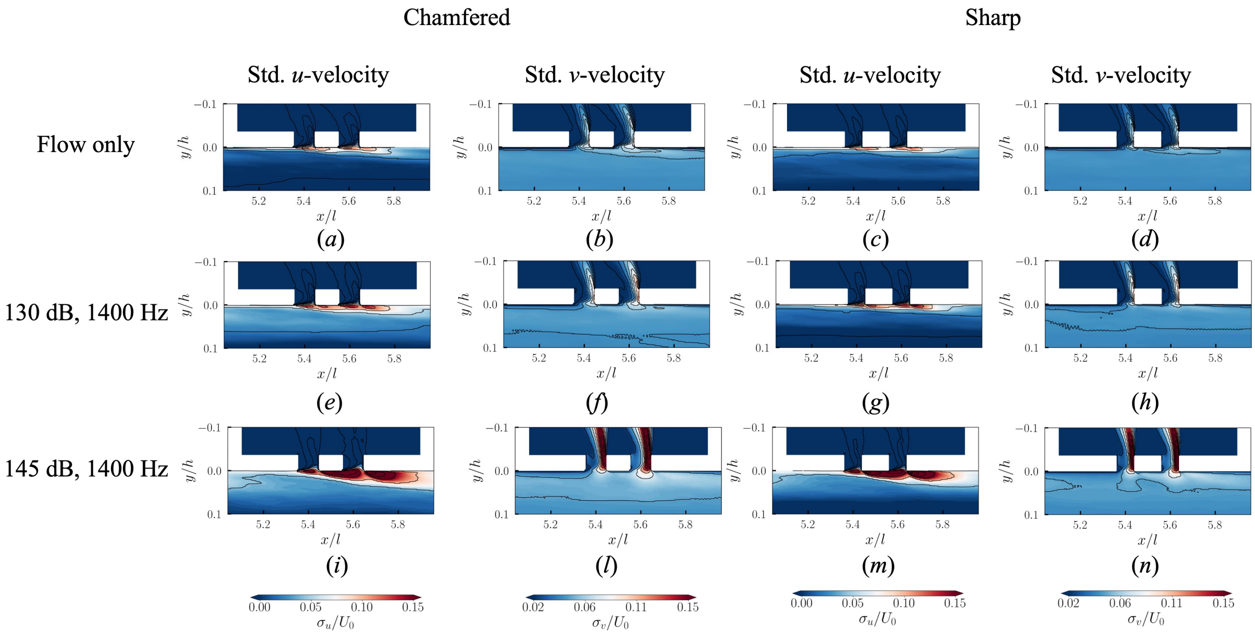

Figure 3. Contours of the standard deviation of the streamwise (a, e, i, c, g, m) and wall-normal (b, f, l, d, h, n) velocity components. Comparison between the chamfered case (a, b, e, f, i, l) and the sharp one (c, d, g, h, m, n) at different SPLs at 1.4 kHz.

higher drag measured for this specific orifice geometry.

2.3 Mean velocity profiles

The mean velocity profiles in wall units downstream of the liner are shown in Figure 4. In both configurations, a clear downward shift ΔU^+ relative to the smooth-wall law of the wall is observed, directly reflecting the increase in drag induced by the liner. This shift is characteristic of rough-wall surfaces and indicates an enhanced momentum deficit in the near-wall region. The magnitude of the shift increases with SPL for both geometries, indicating that acoustic forcing not only affects the global friction coefficient but also modifies the mean velocity profile. At high SPL, the interaction between the grazing flow and the acoustically driven flow within the orifices reduces the streamwise momentum downstream of the orifices. This results in a decrease in the mean velocity and a corresponding increase in the displacement thickness, as reported by Paduano *et al.* (2025).

The influence of frequency on the mean velocity profiles is less pronounced, as shown in Figure 4(c,d). While all cases exhibit a clear downward shift relative to the smooth-wall profile, variations with frequency remain moderate. This suggests that, although frequency affects the unsteady response of the liner, its impact on the mean velocity profile is secondary compared to that of the forcing amplitude.

A systematic difference is observed between the two geometries: the chamfered configuration consistently exhibits a larger downward shift than the sharp-edged one. This behaviour is consistent with the higher drag levels previously reported and indicates that the orifice shape and the consequent enhanced porosity strongly influence the in-orifice and near-wall flow dynamics. The chamfered geometry promotes stronger interaction between the grazing flow and the cavity flow, leading to enhanced momentum exchange and a larger deficit in the mean velocity profile.

To summarize the downward shift of the logarithmic region, Figure 5 presents ΔU^+ as a function of the inverse Forchheimer coefficient for different SPLs, porosities, and frequencies, following the approach proposed by Shahzad *et al.* (2023*a*). The Forchheimer coefficient for each configuration is estimated using Eq. 1.

A first important observation is that ΔU^+ increases as the Forchheimer coefficient decreases. This trend is consistent with previous findings in the literature (Shahzad *et al.*, 2022) and aligns with the physical interpretation of the Forchheimer coefficient: lower values correspond to stronger flow inertial effect within the orifices, leading to enhanced momentum exchange between the cavity flow and the grazing flow and, consequently, a larger downward shift of the mean velocity profile.

For both geometries, the flow-only cases exhibit a nearly constant offset with respect to the reference data of Shahzad *et al.* (2022). This discrepancy may be attributed to the fact that, in the present study, the Forchheimer coefficient is estimated from geometric parameters rather than directly obtained from dedicated measurements or simulations, which may introduce systematic differences in its value. Nevertheless, the overall trend remains consistent.

When acoustic forcing is introduced, the ΔU^+ further departs from the scaling, and the results proposed by Shahzad *et al.* (2023*a*). In particular, for increasing SPL (Figure 5(a)), ΔU^+ increases even for similar values of the Forchheimer coefficient, indicating that acoustic effects enhance the momentum transfer beyond what is predicted by the purely hydrodynamic resistance. By contrast, the frequency dependence (Figure 5(b)) is weaker, although a slight increase of ΔU^+ with frequency can still be observed.

These results indicate that the Forchheimer coefficient, when defined solely from geometric porosity, is insufficient to characterise the drag behaviour under acoustic forcing. While it provides a reasonable scaling for the flow-only case, it fails to collapse the data when acoustic excitation is present. This deviation highlights that the effective resistance of the liner is not purely geometric but depends on the dynamic interaction between the acoustic field and the flow within the orifices. In particular, the unsteady jetting induced by acoustic forcing introduces additional momentum transfer mechanisms that are not captured by classical porous-media models.

A further step would be to correct the Forchheimer coeffi-

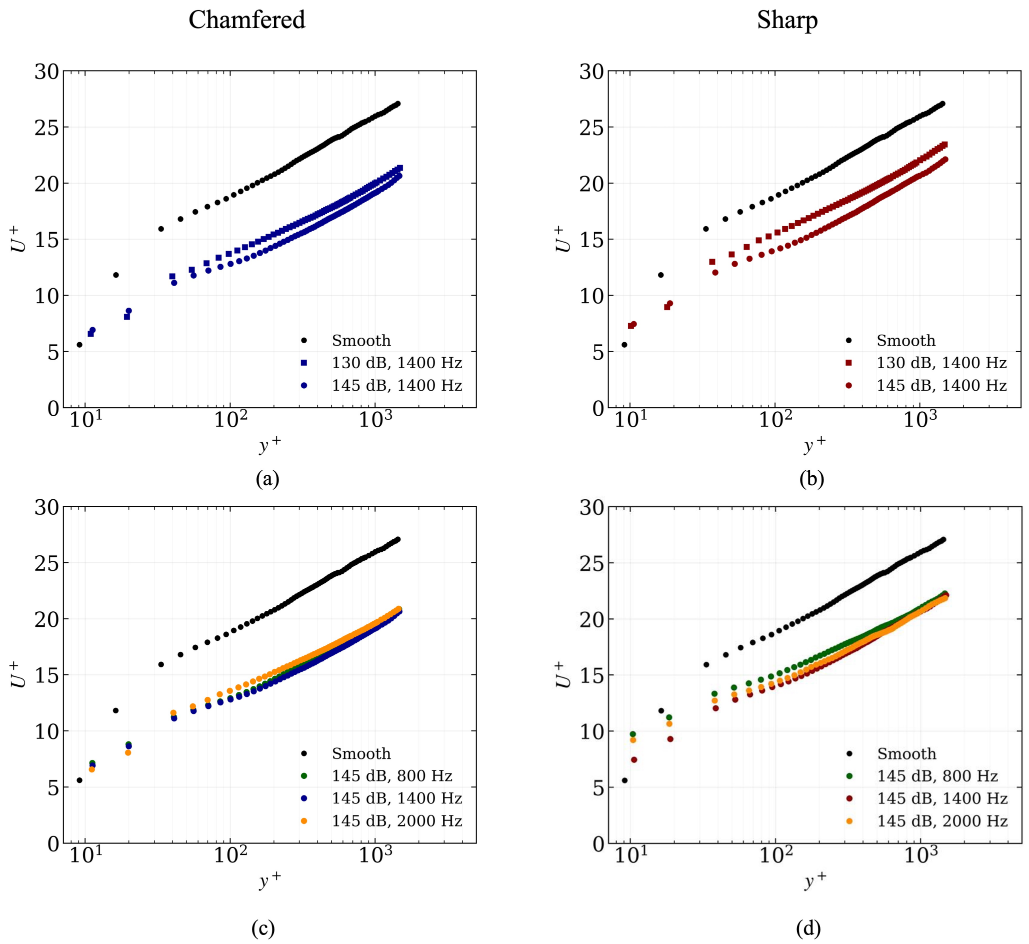

Figure 4. Mean velocity profiles in wall units downstream of the liner. Effect of SPL (a, b) and frequency (c, d). Sharp-edged geometry (b, d) chamfered-edged geometry (a, c).

cient by accounting for the modification of the effective porosity induced by the grazing flow, which has been shown to affect the discharge coefficient (Paduano *et al.*, 2025). This suggests that extensions of the Forchheimer framework, incorporating unsteady and acoustic effects, may be required to accurately predict the aerodynamic performance of liners under realistic operating conditions.

3 Conclusion

Very large eddy simulations have been performed to investigate the aerodynamic penalty induced by acoustic liners subjected to grazing turbulent flow at Mach 0.32 and to incident plane acoustic waves of varying amplitude and frequency. The results provide a preliminary picture of the effect of coupled flow–acoustic mechanisms on the drag increase over perforated surfaces.

The presence of the liner alone produces a substantial increase in drag compared to a smooth wall. Among the geometric parameters, the effective diameter exposed to the grazing flow and the associated increase in porosity have the strongest impact on the drag. In particular, the chamfered configuration consistently exhibits higher drag levels, due to enhanced interaction between the grazing flow and the cavity flow.

When acoustic forcing is introduced, the aerodynamic response becomes strongly dependent on the forcing amplitude. At moderate excitation levels (130 dB), the drag increase remains limited, with an additional rise of less than 4% compared to the flow-only condition, indicating that the acoustic field has a minor impact on the mean flow. In contrast, at high excitation levels (145 dB), a pronounced increase in drag is observed, with an additional rise of up to 12% relative to the flow-only case, associated with a substantial modification of the near-wall turbulence structure.

The flow analysis reveals that this behaviour can potentially be driven by unsteady flow exchange through the orifices. Acoustic forcing induces periodic enhancement of wall-normal velocity fluctuations and promotes stronger coupling between the inner and outer regions of the turbulent flow. This manifests as a downward shift of the velocity profile, analogous to that observed over rough surfaces, although here the effective roughness is dynamically controlled by the acoustic forcing.

The analysis of the mean velocity shift further shows that classical scaling based on the Forchheimer coefficient provides a reasonable description for the flow-only case but fails when acoustic forcing is present. This breakdown indicates that the effective resistance of the liner is not solely determined by its geometric properties, but also depends on the unsteady flow–acoustic interaction within the orifices. Consequently, models based on steady porous-media analogies are insufficient to fully describe the aerodynamic behaviour of liners under realistic operating conditions.

Overall, the present study demonstrates that acoustic liners operating under grazing turbulent flow cannot be assessed solely on the basis of their acoustic performance. The coupling between acoustic waves and turbulence introduces additional

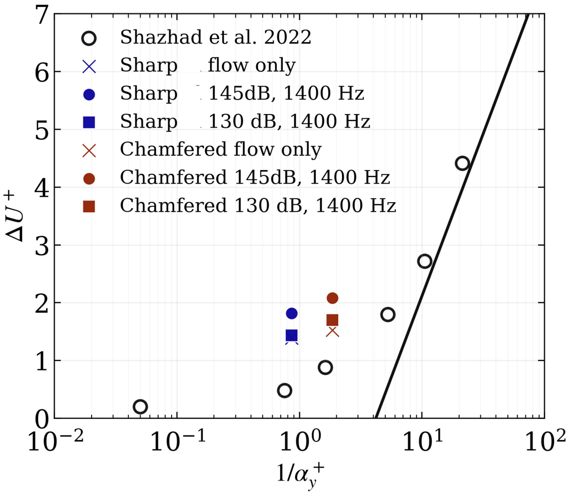

(*a*)

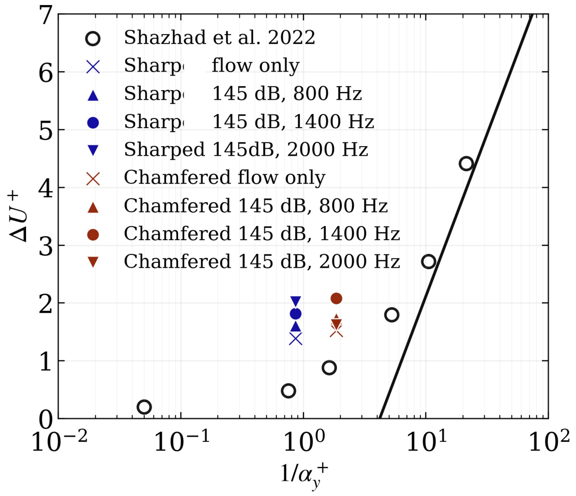

(*b*)

Figure 5. ΔU^+ as a function of the inverse Forchheimer parameter. (a) Effect of the SPL and (b) effect of the frequency.

mechanisms that can significantly increase drag, particularly at high SPL and near resonance conditions. These findings highlight the need for design strategies that account for both acoustic attenuation and aerodynamic penalties, and point towards the development of modelling approaches that incorporate the dynamic interaction between flow, geometry, and acoustic excitation.

Funding: The work of A.P., F.S. and F.A. is co-funded by the European Union (ERC, LINING, 101075903). Views and opinions expressed are, however, those of the author(s) only and do not necessarily reflect those of the European Union or the European Research Council. Neither the European Union nor the granting authority can be held responsible for them.

REFERENCES

Avallone, F., Khedr, A., Paduano, A., Scarano, F., Pereira, L. & Cordioli, J. 2026 On the relevance of facesheet orifice geometry to acoustic liner impedance. *npj Acoustics* **2**.

Bento, H. F. M., Vandercreek, C. P., Avallone, F., Ragni, D. & Snellen, M. 2022 Lattice boltzmann very large eddy simulations of a turbulent flow over covered and uncovered cavities. *Physics of Fluids* **34**.

Bonomo, L. A., Quintino, N. T., Spillere, A. M.N., Cordioli, J. A. & Murray, P. B. 2022 A Comparison of In-Situ and Impedance Eduction Experimental Techniques for Acoustic Liners with Grazing Flow and High SPL. In *28th AIAA/CEAS Aeroacoustics Conference, 2022*.

Chung, D., Hutchins, N., Schultz, M. P. & Flack, K. A. 2021 Predicting the drag of rough surfaces. *Annual Review of Fluid Mechanics* **53** (Volume 53, 2021), 439–471.

de Giovanetti, M., Hwang, Y. & Choi, H. 2016 Skin-friction generation by attached eddies in turbulent channel flow. *Journal of Fluid Mechanics* **808**, 511–538.

He, X. & Luo, L. S. 1997 Theory of the lattice Boltzmann method: From the Boltzmann equation to the lattice Boltzmann equation. *Physical Review E - Statistical Physics, Plasmas, Fluids, and Related Interdisciplinary Topics* **55** (6).

Howerton, B. M. & Jones, M. G. 2016 Acoustic liner drag: Measurements on novel facesheet perforate geometries. In *22nd AIAA/CEAS Aeroacoustics Conference, 2016*.

Idelchik, I. E. 1986 *Handbook of hydraulic resistance (2nd revised and enlarged edition)*.

Jasinski, C. & Corke, T. 2020 Mechanism for increased viscous drag over porous sheet acoustic liners. *AIAA Journal* **58** (8), 3393–3404.

Paduano, A., Scarano, F., Cordioli, J., Casalino, D. & Avallone, F. 2025 On the impact of the turbulent grazing flow development on the acoustic response of an acoustic liner. *arXiv preprint arXiv:2507.22714* .

Paduano, A., Scarano, F., Cordioli, J., Casalino, D. & Avallone, F. 2026 n the impact of the orifice shape in acoustic liner attenuation under turbulent grazing flow. In *32th AIAA/CEAS Aeroacoustics Conference (2026)*.

S., Francesco, J., Marc C. & G., Erwin R. 2023 Drag reduction by means of an array of staggered circular cavities at moderate reynolds numbers. *International Journal of Heat and Fluid Flow* **102**, 109142.

Scarano, F., Jacob, M. C. & Gowree, E. R. 2024 Large scale structures modification of a spatially evolving turbulent boundary layer grazing over circular cavities. *International Journal of Heat and Fluid Flow* **108**, 109486.

Schultz, M. P. & Flack, K. A. 2013 Reynolds-number scaling of turbulent channel flow. *Physics of Fluids* **25**.

Shahzad, H., Hickel, S. & Modesti, D. 2022 Permeability and turbulence over perforated plates. *Flow, Turbulence and Combustion* **109**, 1–14.

Shahzad, H., Hickel, S. & Modesti, D. 2023*a* Direct Numerical Simulation of a Turbulent Boundary Layer over Acoustic Liners. American Institute of Aeronautics and Astronautics (AIAA).

Shahzad, H., Hickel, S. & Modesti, D. 2023*b* Turbulence and added drag over acoustic liners. *Journal of Fluid Mechanics* **965**.

Shahzad, H., Hickel, S. & Modesti, D. 2025 Direct numerical simulation of a turbulent boundary layer over acoustic liners. *AIAA Journal* **63** (11), 4650–4661.

Tam, C. K.W., Pastouchenko, N. N., Jones, Michael G. & Watson, W. R. 2014 Experimental validation of numerical simulations for an acoustic liner in grazing flow: Self-noise and added drag. *Journal of Sound and Vibration* **333**.

Tam, C. K. W. & Kurbatskii, K. A. 2000 Microfluid Dynamics and Acoustics of Resonant Liners. *AIAA Journal* **38** (8), 1331–1339.

Texeira, C. M. 1998 Incorporating turbulence models into the Lattice-boltzmann method. *International Journal of Modern Physics C* **9** (8).

Yakhot, V. & Orszag, S. A. 1986 Renormalization-group analysis of turbulence. *Physical Review Letters* **57** (14).